Oceanologia (2021) 63, 27—39

Available online at www.sciencedirect.com

ScienceDirect

journal homepage: www.journals.elsevier.com/oceanologia

ORIGINAL RESEARCH ARTICLE

Assessment of wave energy in the Persian Gulf: An evaluation of the impacts of climate change

Hamid Goharnejad[a,b,*], **Ehsan Nikaein**[a], **Will Perrie**[b]

[a] *Department of Civil Engineering, Environmental Sciences Research Center, IslamShahr Branch, Islamic Azad University, IslamShahr, Iran*
[b] *Fisheries and Oceans Canada, Bedford Institute of Oceanography, Dartmouth, Nova Scotia, Canada*

Received 31 January 2020; accepted 9 September 2020
Available online 28 September 2020

KEYWORDS
Wave energy potential;
RCP8.5;
RCP4.5;
Persian gulf;
Mike SW

Abstract We are motivated to study the exploitation of marine energy as a renewable resource because of society's ever-increasing energy demands, and a concomitant need to reduce greenhouse gas emissions. Additionally, climate-related variations in wave energy should be investigated in order to ensure the stability of its long-term availability. Here, we investigate the potential for wave energy in the Persian Gulf along the southern coasts of Iran. To do so, we have applied the Mike SW numerical model and ECMWF wind field data for a 30-year study, from 1988 to 2017. For this purpose, wave energy was evaluated at six points in the western, northern, southern, and eastern parts of the Persian Gulf. To assess the impacts of climate change, we also consider the wave regime from 2070 to 2099 (for 30 years) following IPCC RCP4.5 and RCP8.5 climate change scenarios. Our findings suggest that in the present climate, seasonal variations in the mean wave parameters (i.e. wave energy, wave period, and significant wave height) correspond to the lowest wave energy in the summers, and highest in the winters. In the future climate change scenarios, energy level variations generally have similar patterns, with slight modulations in some local areas.

* Corresponding author at: Department of Civil Engineering, Environmental Sciences Research Center, IslamShahr Branch, Islamic Azad University, IslamShahr, Iran.
E-mail addresses: hgn1982@gmail.com (H. Goharnejad), nikaein_e@yahoo.com (E. Nikaein), william.perrie@dfo-mpo.gc.ca (W. Perrie).
Peer review under the responsibility of the Institute of Oceanology of the Polish Academy of Sciences.

Production and hosting by Elsevier

https://doi.org/10.1016/j.oceano.2020.09.004

1. Introduction

According to the Implementation Agreement on Ocean Energy Systems (2007), the global ocean wave energy is estimated at approximately 93100 TWh/yr. Therefore, in recent years extensive studies have been completed on wind-wave energies in the global ocean and coastal seas, and the potential for wave energy extraction (Besio et al., 2016; Kumar and Anoop 2015; Neil and Hashemi, 2013). A lot of studies have been completed to assess the wave energy potential around the world (Alonso et al., 2015; Appendini et al. 2015; Gallagher et al., 2016; Jadidoleslam et al., 2016; Liang et al., 2016; López et al., 2015; Morim al., 2014; Neill et al., 2014; Ponce de León et al., 2016; Rusu and Onea, 2013; Wang et al.; 2016, Zhou et al. 2015a,b). All of these indicate that the use of high precision data is indispensable for assessing the local parameters of wave energy. Therefore, our study is focused on a high accuracy evaluation of the temporal and spatial parameters of waves in coastal areas of the Persian Gulf. In addition, the present and future wind climate must be considered as the main source of wave energy production. Recent research has shown that in the twentieth century, the mean sea level and the average wind speed have increased by 30 cm and 1 m/s, respectively (WCRP, 2018).

Meanwhile, several studies have considered climate change and winds in areas such as the Red Sea (Aboobacker et al., 2017; Langodan et al., 2016; Shanas et al., 2017), the Mediterranean Sea (Kapelonis et al., 2015), and the Caspian Sea (Amirinia et al., 2017), the Persian Gulf and Oman sea (Armanfar et al., 2019; Goharnejad et al., 2013) for a variety of purposes, including wave energy assessment and climate change impacts. Also, the IPCC climate change scenarios, specifically RCP8.5 emissions scenarios for the end-of-century period (2081—2100), suggest that mean wind speeds will decrease in the North Atlantic, but increase in the Southern Hemisphere, and thus that the wave climate may experience higher wave heights in these areas. These changes will increase the peak periods of the waves, for example in the eastern South Pacific Ocean and the Indian Ocean, causing the mean wave direction to tend to experience counterclockwise rotation in southern oceans (Casas-Prat et al., 2018).

Vieira et al. (2020) studied wave climate-energy patterns for different seasons for the Persian Gulf and found that waves during winter and springtime are more energetic, and become milder in the autumn. Alizadeh et al. (2020) showed a decreasing trend for the overall Persian Gulf, which is relatively severe in northern areas and has an impact on the potential for future wave energy. In the Persian Gulf, the mean significant wave height has greater variability than that of wind speed, although the dominant wave direction has greater stability than that of wind direction (Kamranzad, 2018). Kamranzad et al. (2017) compared two stations in the northern Persian Gulf, at Asalouyeh and Boushehr, and found that the sustainability for wave energy and harvesting is higher at the former, compared to the latter. Moreover, Kamranzad et al. (2015) suggest that the annual wave energy will decrease at both stations for A2, B1, and A1B climate change scenarios. In terms of the present climate, for the period from 1984 to 2008, Kamranzad et al. (2013) investigated the wave energy characteristics at three locations in the Persian Gulf (western, central and eastern) and report that both seasonal and decadal variations can be seen in the wave energy trends, on account of present climate variability.

The focus of this study is the wave climate in the Persian Gulf, motivated by the potential for exploitation of renewable wave energy. An assessment of wave climate in this area suggests that the most significant wave heights should occur in the central part of the Persian Gulf in January and February (Kamranzad and Chegini, 2014).

In this paper, we assessed the potential wave energy for the Persian Gulf area. Although, a wide range of research has been completed in this study area, consideration has not been given to climate change impacts according to the latest scenarios, RCP8.5 and RCP4.5. Moreover, in this research, we almost tried to assign a 'Wave Energy Development Index' as an indicator of potential energy development. Finally, we provide a 'bivariate probability distribution of occurrence' and wave energy matrices.

2. Study area

The Persian Gulf is formed as an extension of the Indian Ocean, with an area of 237,473 square kilometers, and following the Gulf of Mexico and the Hudson Bay, is the third largest bay in the world. The Persian Gulf runs from the waters east of the Strait of Hormuz and the Oman Sea to the Indian Ocean and the Arabian Sea. According to a previous sensitivity analysis completed in this study area by Liao and Kaihatu (2016), the impacts of the boundary waves at the Oman Sea on wind-waves in the Persian Gulf are negligible; therefore no wave spectral are specified as outer boundary conditions. The Gulf's geographic coordinates are from 24° to 30°30'N and from 48° to 56°25'E of the Greenwich meridian. The length of the Persian Gulf from the Strait of Hormuz to its most western location is about 805 kilometers. At its widest, the Gulf is 290 kilometers. The maximum depth of the Persian Gulf is 93 meters and the shallowest waters are about 10—30 meters in the western part. There are several islands in the Gulf. In terms of topography (Figure 1), the Persian Gulf is asymmetrical and the slopes of its southern coasts are milder than the slopes of its northern shores (Pous et al., 2015).

3. Material and methods

3.1. Spectral wave model setup and wave data

In order to study the wave regimes in the Persian Gulf, it is necessary to specify bathymetry data, wind speeds and directions, buoy wave data, and sea level pressure data. In this study, the Spectral Wave (SW) model component of the MIKE modeling system (DHI, 2005) is used in order to hindcast the wave characteristics, driven by wind climate data. Waves are numerically modeled using the SW model, a dynamic modeling system based on the SWAN spectral wave model, which is implemented on an irregular unstructured grid. For more details about the unstructured grid mesh, see Korn (2017). The SW model solves the energy transfer

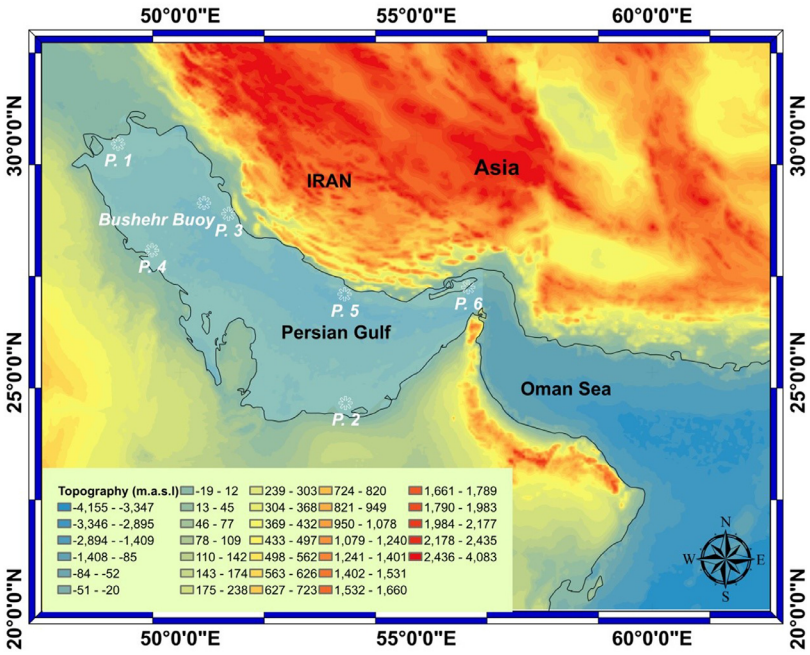

Figure 1 Location of selected points in the Persian Gulf.

equation including source and sink terms to predict the developing wave field.

The SW governing wave model equation is the spectral action balance equation, which in Cartesian coordinates is:

$$\frac{\partial}{\partial t}N + \frac{\partial}{\partial x}C_{g,x}N + \frac{\partial}{\partial y}C_{g,y}N + \frac{\partial}{\partial \sigma}C_{g,\sigma}N + \frac{\partial}{\partial \theta}C_{g,\theta}N = \frac{S}{\sigma}, \quad (1)$$

where σ is the relative frequency, θ is wave direction, N is wave action density, which is equal to the energy density divided by the relative frequency ($N(\sigma, \theta) = E(\sigma, \theta) / \sigma$), and C_g is the propagation velocity of wave action in (x, y, σ, θ) space. The last term on the left side of Eq. (1) represents the effects of refraction and shoaling. The source term on the right side is defined as:

$$S = S_{in} + S_{nl} + S_{dis} + S_{ot} + S_{surf}, \quad (2)$$

where S_{in} represents energy transfer from the wind to the waves, S_{nl} is the energy transferred from one frequency to other frequencies by nonlinear wave-wave interactions, S_{dis} is wave dissipation due to the effects of white-capping, S_{ot} is the wave dissipation due to bottom friction, and S_{surf} represents wave dissipation resulting from the wave breaking in a shallow area.

3.2. Model implementation

Bathymetry must be specified in order to use the SW model to simulate waves. This is achieved by implementing gridded bathymetric data at 30 arc-second intervals in the north/south latitudinal direction and also the east/west longitudinal direction, as provided by the British Oceanographic Data Center (BODC), as extracted from gebco.net. The bathymetric chart and unstructured mesh of the study area, including 17000 meshes and 8670 nodes, are presented in Figure 2 (A and B, respectively).

Table 1 Specifications for Boushehr buoy in the Persian Gulf.

Station Name	Latitude (°N)	Longitude (°E)	Water depth (m)
Boushehr	28.58	50.5	28

One of the important inputs for this model is the wind field data. For this purpose, data from the European Center for Medium-Range Weather Forecasts (ECMWF) was used in this study. The ECMWF ERA-interim wind field data was extracted from http://apps.ecmwf.int with 0.125 × 0.125 degrees spatial resolution in the study zone and 6-hourly time interval.

A sensitivity analysis of dissipation parameters due to white capping, bottom friction, and depth induced wave breaking was carried out, which suggests that the white capping factor is effectively the dominating factor.

3.3. Spectral wave model performance

In order to evaluate the model performance, the model is implemented using available data for particular case studies. After analyzing the sensitivity of its' parameters to observed field data (calibration), the model is implemented for additional conditions and the results are compared with more field data to estimate model accuracy (validation). In the present study, the model is implemented for two 6-month periods while varying the effective parameters. Table 1 presents the specifications of the Boushehr buoy in the study area.

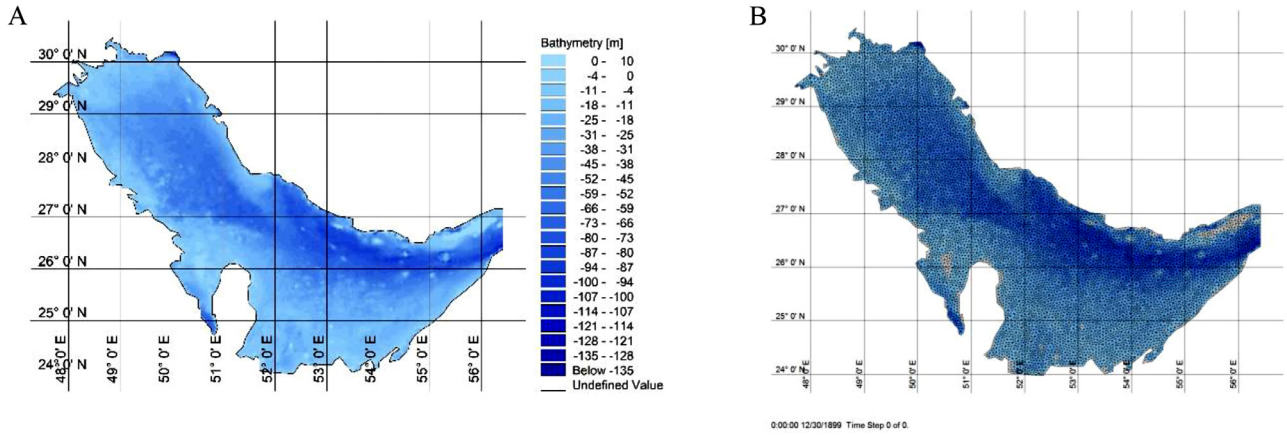

Figure 2 A) Bathymetry data, and B) triangular meshes including 17000 meshes and 8670 nodes in the study area.

Table 2 Model performance indices for the Boushehr buoy.

Parameter	Normal Range	Ideal Range	Calibration	Validation
Bias (m)	0.2–0.5	<0.3	0.22	0.20
CC	0.75–0.90	>0.8	0.79	0.82
RMSE(m)	0.1–0.7	<0.5	0.40	0.35
SI	0.15–0.35	<0.3	0.23	0.16

Statistical parameters between observed and modeled data are calculated:

Bias $\quad \text{Bias} = \left(\bar{S} - \bar{O}\right), \tag{3}$

Root mean squared errors $\quad \text{RMSE} = \sqrt{\frac{1}{N}\sum (S_i - O_i)^2}, \tag{4}$

Correlation coefficient $\quad \text{CC} = \frac{\sum \left(S_i - \bar{S}\right)\left(O_i - \bar{O}\right)}{\sqrt{\sum \left(S_i - \bar{S}\right)^2 \sum \left(O_i - \bar{O}\right)^2}}, \tag{5}$

Dispersion coefficient $\quad \text{SI} = \frac{\sqrt{\frac{1}{n}\sum \left(\left(S_i - \bar{S}\right) - \left(O_i - \bar{O}\right)\right)^2}}{\bar{O}}, \tag{6}$

where O_i is the observed value at the i^{th} time step, S_i is a forecast value at the same time, N is the number of time steps and $\bar{O}$ and $\bar{S}$ is the mean value of the observed data. Table 2 presents results for the model performance, with columns 2 and 3 giving the normal and ideal ranges for each performance index. These results suggest that the SW model is sufficiently accurate to use for wave climate estimates in this study. Associated values for modeled and observed significant wave heights (H_s) are presented in Figure 3 and 4 as a calibration and validation periods.

For calibration and validation, two 6-month periods are selected from March 7, 2015 to September 7, 2015 and from September 8, 2015 to March 7, 2016, respectively. These periods are chosen because they contain the best performance times of the buoy with minimal data gaps.

3.4. Evaluation of wave energy

The wave estimates obtained from the SW model are used to estimate wave power potential in the study area. Several methods are presented by Ertekin and Yingfan (1994) to estimate wave power using H_s and wave period, T. The mean wave energy density per unit horizontal area (J/m^2) is calculated as:

$$E = \frac{1}{16}\rho g H_s^2 \tag{7}$$

in which ρ is the seawater density (kg/m^3), g is the gravity (m/s^2) and H_s is the significant wave height (m). The wave power is expressed as:

$$P = ECn, \tag{8}$$

where C is the wave speed (m/s) and n is the ratio of the wave group speed and wave speed. C is equal to the wavelength divided by the wave period (T) and is equal to $\frac{gT}{2\pi}$. The approximate value of n is 0.5 in deep water. Therefore, the wave power is calculated as:

$$P = \frac{1}{16}\rho g H_s^2 \times \frac{gT}{2\pi} \times 0 \cdot 5 \approx 0 \cdot 49 H_s^2 T. \tag{9}$$

3.5. Impact of climate change

In their Fifth Assessment Report (AR5), the Intergovernmental Panel on Climate Change (IPCC) has adopted several Representative Concentration Pathways (RCP) scenarios as possible greenhouse gas concentration pathways that might dominate the future climate. Four pathways have been labeled as RCP2.6, RCP4.5, RCP6, and RCP8.5, which indicate the possible radiative forcing values by the end-of-century, 2100 (Allen et al., 2014).

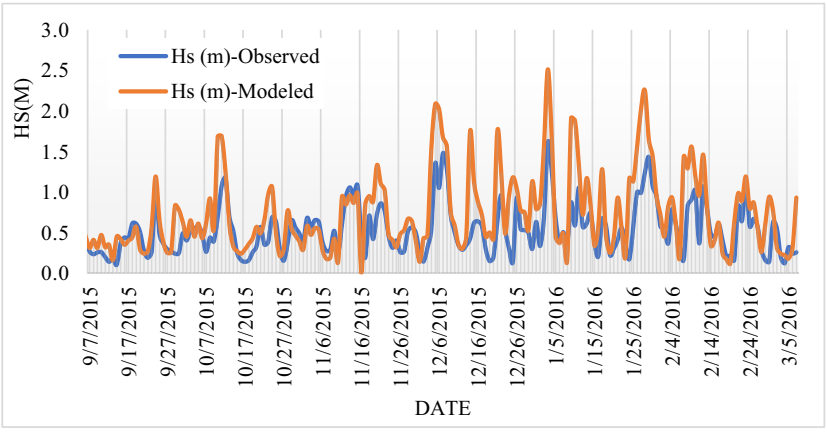

Figure 3 Comparison of modeled and buoy-observed significant wave heights (H_s) time series during the calibration period (8 March 2015 to 7 September 2015).

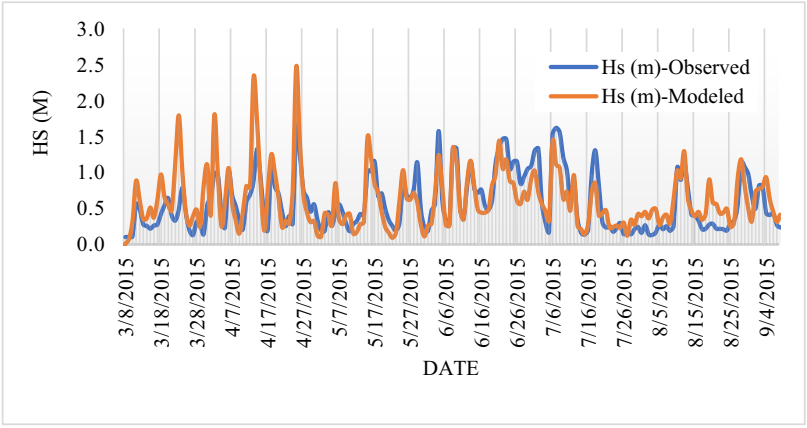

Figure 4 As in Figure 3, comparison of modeled and buoy-observed H_s time series during the validation period (7 September 2015 to 7 March 2016).

RCP8.5 assumes a comparatively high greenhouse gas emissions pathway, associated with the implementation of no effective global climate change mitigation policies or measures, leading to a radiative forcing of 8.5 W/m^2 by the end-of-century. At that time, carbon dioxide concentrations can be expected to reach 1000 ppm and continue increasing (Riahi et al., 2011). RCP4.5 scenario assumes a stabilizing of the radiative forcing at 4.5 W/m^2 by 2100 (Thomson et al., 2011).

In this study, climate change data are extracted from HadGEM2-AO_r1i1p1 (http://apdrc.soest.hawaii.edu/data/data.php). HadGEM2 is a coupled Earth System Model that was used by the Met Office Hadley Centre for the CMIP5 centennial simulations. On account of the large spatial and temporal scales of climate change data, downscaling should be implemented to translate the coarse-resolution HadGEM2 outputs to finer resolution climate information. In particular, the data resolution for HadGEM2 is not appropriate for modeling wave regimes in the Persian Gulf; for example, monthly time steps in climate change model outputs need to be downscaled to hourly data. In this research, a combination of dynamical and statistical approaches is applied, namely the so-called 'change factor method' which was used by Kamranzad et al. (2015) for the Persian Gulf to evaluate wind/wave power, and by Breslow and Sailor (2002) in USA applications for wind power estimates.

The approach of hybrid dynamical-statistical downscaling can be considered as a challenge to use the potential of dynamical downscaling to prepare fine-scale climate changes along with the advantages of statistical downscaling. In this study, we used a dynamical-statistical downscaling technique used by Kamranzad et al. (2015).

In order to assess the dependability of outputs of the climate models, observed data and climate model data are compared over the entire study area. Thus, control periods are specified and selected locations are tested. Underestimates in wind data for climate change scenarios can be identified by comparisons between ECMWF and HadGEM2 data. Biases in climate change wind data are corrected by application of modification coefficients introduced by Kamranzad et al. (2015) for CGCM3.1 using a hybrid method, defined in terms of the monthly averages of absolute wind components, estimated as:

$$\beta_u = \frac{|u|_{\text{ECMWF(monthly average)}}}{|u|_{\text{HadGEM2(monthly average)}}}, \tag{10}$$

$$\beta_v = \frac{|v|_{\text{ECMWF(monthly average)}}}{|v|_{\text{HadGEM2(monthly average)}}}, \tag{11}$$

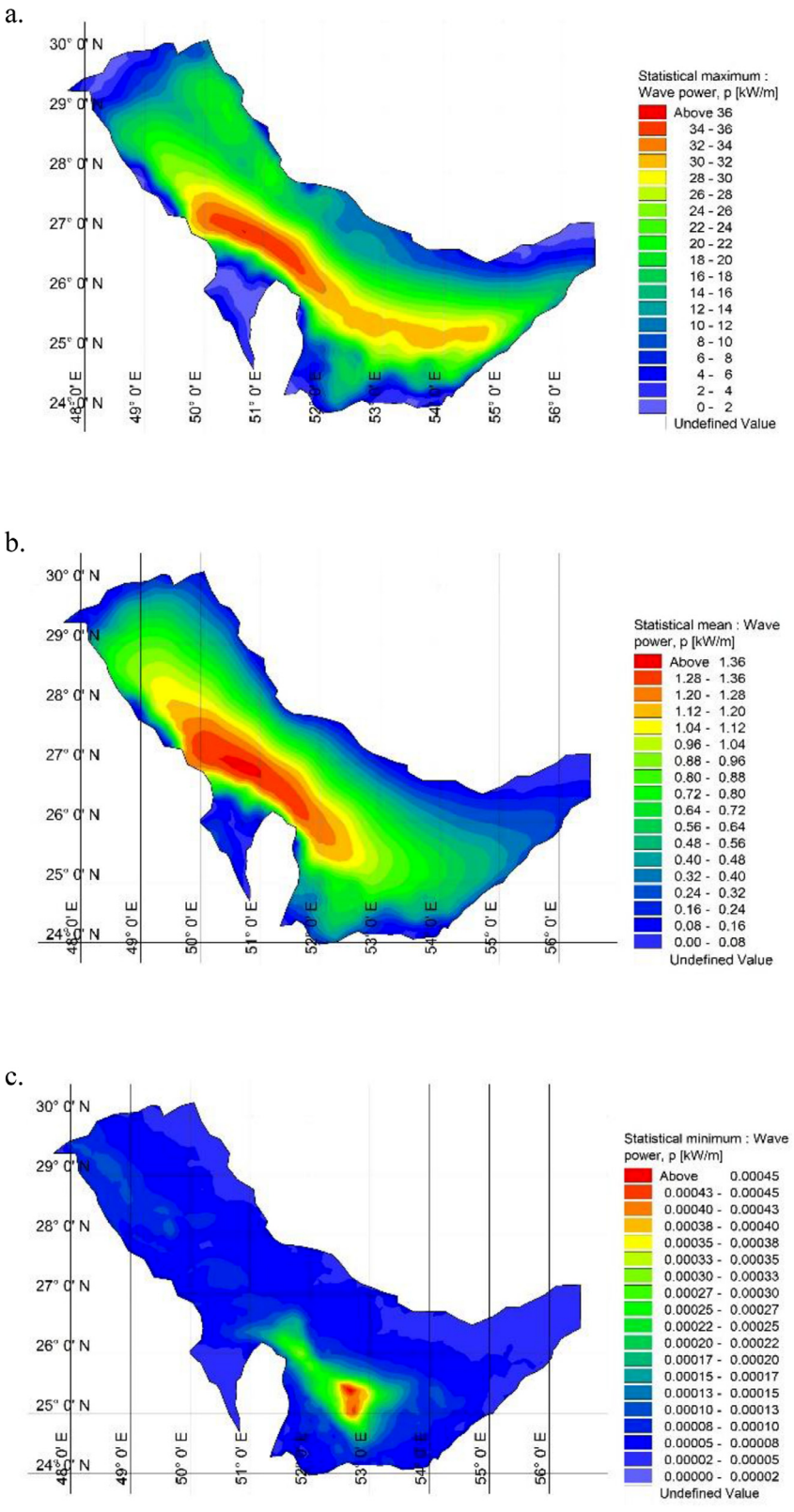

Figure 5 (a) Maximum, (b) mean, and (c) minimum wave energy for 30 years (1988–2017).

where β_u and β_v represent the modification factors for u and v components of the wind speed, respectively.

Thus, the ratios of directional wind speed data between ECMWF and HadGEM2, for scenarios RCP4.5 and RCP8.5, can be shown to vary between 1.15 to 2.15, and 1.25 to 2.30, respectively. Once climate change wind speed data were downscaled and corrected, the spectral wave model was run for 30-year periods of future scenarios (2070–2099).

3.6. Wave Energy Development Index

Extreme Value Analysis (EVA) and a corresponding Wave Energy Development Index (WEDI) can be used to assess the level of severity at a given spatial location. WEDI can estimate the potential hazards that may occur in terms of extreme events at Wave Energy Converters (WECs) and offshore structures:

$$\mathrm{WEDI} = \frac{\overline{P_{wave}}}{J_{wave}}, \tag{12}$$

which is the ratio of annual average wave power (P_{wave}) to the maximum storm wave power (J_{wave}). Wave Energy Converters are usually placed at specific locations based on estimates for mean power potential. An additional consideration is the maximum power potential, as well as estimates for the severity of extreme events, penalizing locations with high WEDI index values, as considered by Hagerman (2001).

4. Results and discussion

The time series of H_s and T_p are obtained from the SW model and wave energy is calculated for a period of 30 years (1988–2017) in the present climate, and a 30 years (2070–2099) in the future. Figure 5A–C gives the maximum, average and minimum values for wave energy as simulated for the current period.

In Figure 6, mean yearly wave power changes for historical and future climate time-periods are shown. Calculations of the trends demonstrate that there is an ascending trend for the historical period, while both climate change scenarios have descending trends and the trend for RCP4.5 is milder.

4.1. Seasonal variations of wave energy

As shown in Figure 5, there are variations in wave energy in the western, northern, eastern and southern parts of the Persian Gulf. To assess potential wave energy in this study area, six points are selected, with regard to spatial distribution, depth and distance to the coastline, labeled 1 to 6 as shown in Figure 1. The characteristics of these locations are given in Table 3.

As shown by Figure 7, the average wave energy level in the present climate increases from the northern part of the Gulf to the southern part. The maximum energy is estimated at point 4, located in the southern Gulf, estimated at approximately 0.33 kW/m. The lowest energy is estimated in the eastern Gulf within the Strait of Hormuz, at approximately 0.08 kW/m.

With respect to RCP4.5 and RCP8.5 climate change scenarios, estimated values for energy follow similar patterns

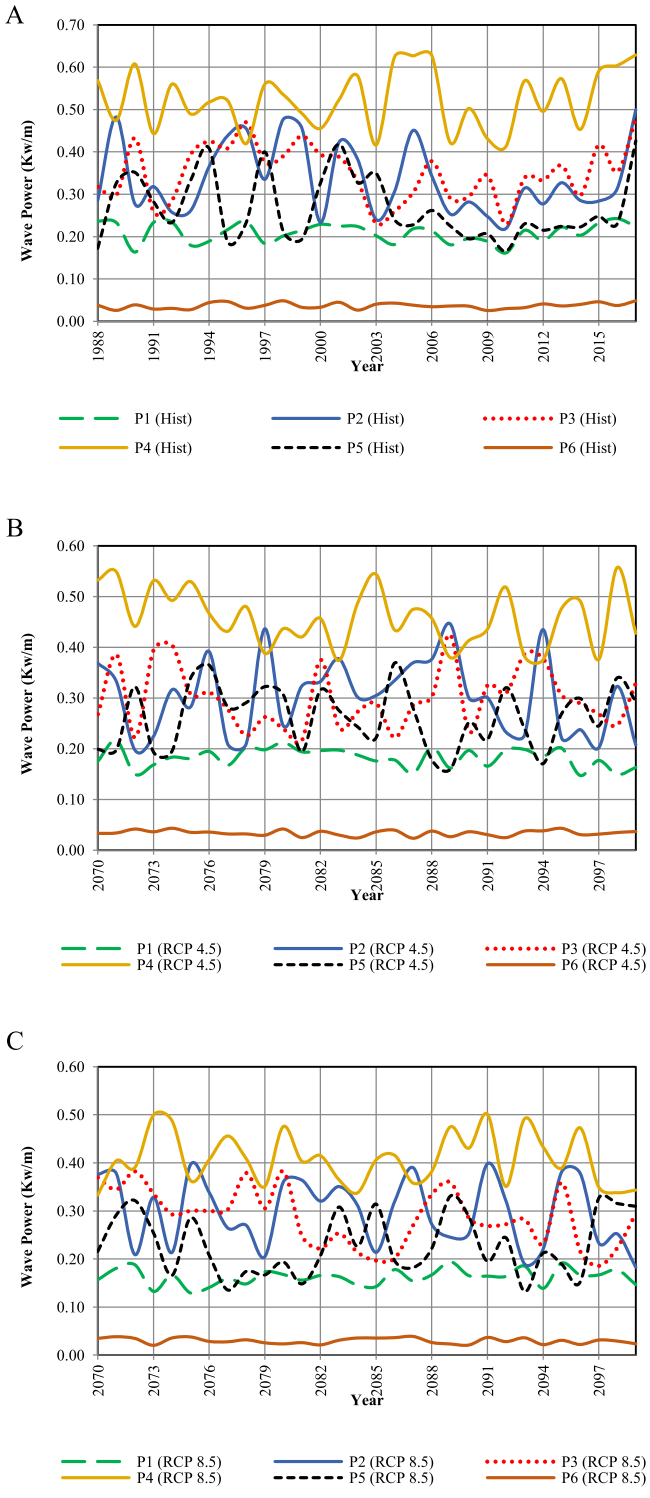

Figure 6 Mean yearly wave energy for 30-year periods: (A) historical period, 1988–2017, (B) climate change scenario RCP4.5, and (C) climate change scenario RCP8.5, 2070–2099.

as for the present climate, implying that although the overall wave energy pattern will not change, in fact, there are significant changes in the amount of generated wave power. Competing effects occur. The extractable energy will increase by about 13–30% at locations 4, 5 and 6, in both RCP4.5 and RCP8.5 climate change scenarios, as shown

Table 3 Characteristics and location of six selected locations.

Point ID	Latitude (° N)	Longitude (° E)	Depth (m)	Position in the Persian Gulf	Maximum Distance from coastline (km)	J_{mean} (kW/m)
1	29.83	48.68	27	North-West	2	0.81
2	24.35	53.50	19	South	2	1.80
3	28.35	51.02	24	North	2	2.00
4	27.58	49.40	19	South	2	2.93
5	26.65	53.48	76	North	2	0.92
6	26.80	56.10	71	North-East	2	0.10

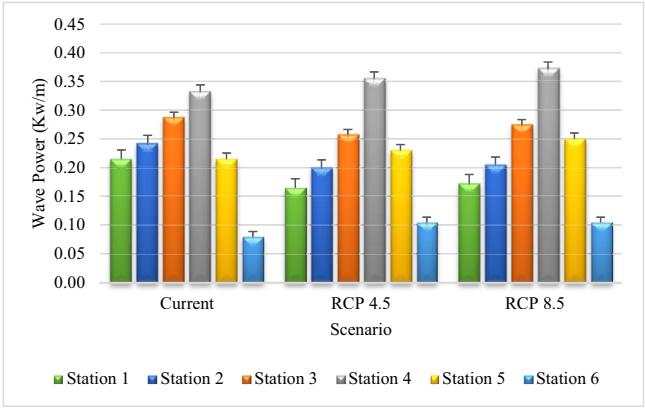

Figure 7 Annual average wave energy at selected stations during 30 years (1988—2017) for RCP8.5 and RCP4.5 climate change scenarios for 30 years (2070—2099).

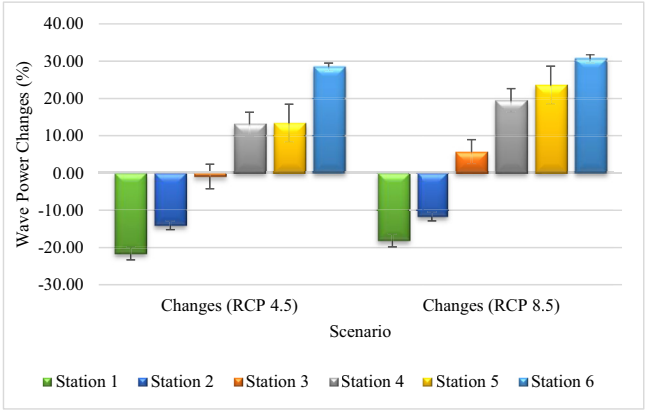

Figure 8 Annual average wave energy changes at selected stations during 30 years (1988—2017) relative to RCP8.5 and RCP4.5 climate change scenarios for 30 years (2070—2099).

in Figure 8. By comparison, at location 3, there will be about 1% reduction in energy in the RCP4.5 scenario, and about 6% more energy, in the RCP8.5 scenario. At stations 1 and 2, there is about 11—21% reduction in energy in both RCP4.5 and RCP8.5 climate change scenarios. Moreover, results have shown that the average wave energy production in the study area is about 0.23 kW/m in the present climate, which compares to 0.22 kW/m and 0.23 kW/m according to the RCP4.5 and RCP8.5 climate change scenarios, respectively. Thus, it is apparent that the negative and positive components in the future climate scenarios may largely cancel each other out.

For the present climate conditions, the directional variations of wave energy are given for the 6 selected locations in Figure 9. Thus it is shown that the dominant wave directions at locations 1, 2, 3, 4, and 5 are from the north and northeast. Also, at location 6 the prevailing energy comes from the northwest, indicating that the Oman Sea has a direct effect on this locality.

4.2. Seasonal wave energy

The average seasonal wave energy is also investigated in this study. As shown in Figure 10, the average wave energy values in winter, spring, autumn and summer are 0.33, 0.24, 0.19, and 0.16 kW/m, respectively. Thus, winter and summer have the highest and lowest wave energy values, respectively. In the RCP4.5 scenario, the maximum amount of energy is expected to be produced in winter, whereas the minimum amount occurs in autumn. In the RCP 8.5 scenario, the wave energy patterns are expected to have the highest variation i.e. the average wave energy in spring, winter, autumn and summer are 0.26, 0.24, 0.22 and 21.0 kW/m, respectively. As Figure 11 shows, the wave energy has a decreasing average in winter, whereas this average value is ascending in the other seasons. The maximum ascending average seasonal wave energy occurs in summer at 26.83 and 28.01 kW/m for the RCP4.5 and RCP8.5 climate change scenarios, respectively.

Therefore, it can be suggested that the mean values in projected changes are more severe in the RCP8.5 scenario than those in the RCP4.5 scenario.

We have also compared wave energies in each season using the 30 years (1988—2017) model results, at selected locations. At location 1 on the western side of the Persian Gulf, the amount of wave energy varies from 0.25 kW/m in winter to 0.18 kW/m in the summer. At location 2 in the southern part of the Persian Gulf, the amount of wave energy varies from 0.33 kW/m to 0.17 kW/m in winter and summer, respectively. Also, in the northwestern Gulf at location 3, the amount of wave energy changes from 0.45 kW/m to 0.20 kW/m in winter and summer, respectively. At location 4 in the southwestern part of the Gulf, the maximum amount of wave energy is observed, changing from 0.48 kW/m in the winter to 0.21 kW/m in the summer. In the northern part of the Gulf at location 5, the amount of wave energy changes from 0.31 to 0.16 kW/m in winter and summer, respectively. Finally, on the eastern side of the Gulf

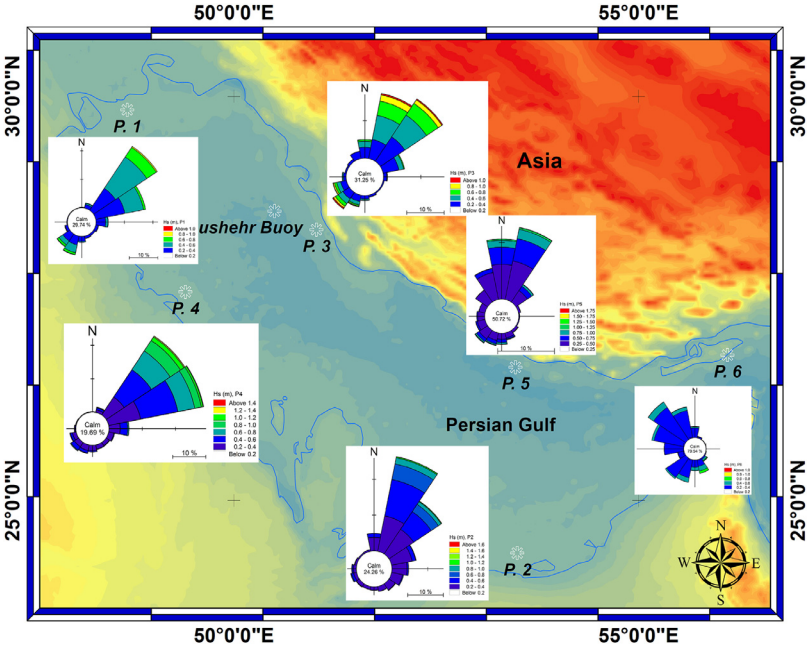

Figure 9 Directional distributions for wave energy at selected locations for the present climate.

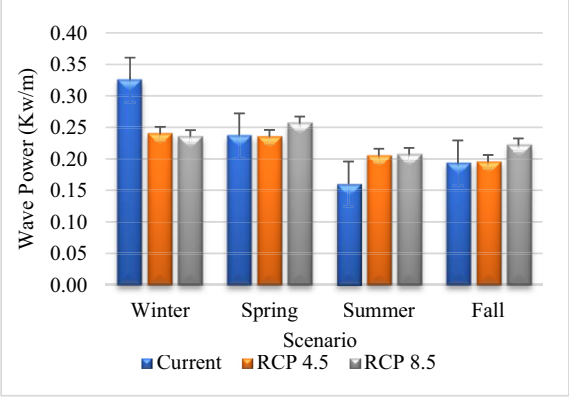

Figure 10 Seasonal mean wave energy at selected locations during 30 years (1988–2017) for the present climate, and for RCP8.5 and RCP4.5 climate change scenarios.

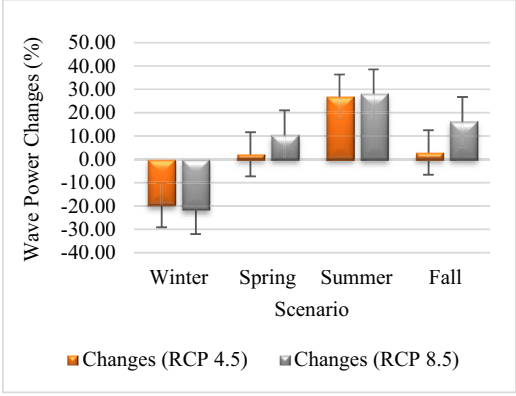

Figure 11 Seasonal mean wave energy changes (%) at selected locations for RCP8.5 and RCP4.5 climate change scenarios relative to the present climate, represented by 30 years (1988–2017).

in the Strait of Hormuz, near the Oman Sea, the minimum amount of wave energy is estimated for location 6, changing from 0.13 in winter to 0.04 kW/m in summer. The reason for this considerable reduction in the wave energy is due to the relatively short fetch in this area. Meanwhile, according to Figure 12(A–D) the amount of wave energy in the spring is higher than in autumn and summer.

According to both RCP4.5 and RCP8.5 climate change scenarios, the prevailing wave energy patterns in the locations that we considered are consistent with the present climate. However, according to Figure 13, these changes do not follow the same averages at all locations. For example at locations 1 and 2, during the winter, spring and autumn, the mean value in wave energy variations shows a downward mean amount and has an increasing average only in summer. At location 3, the mean value in wave energy variations in the winter is descending, for both scenarios of climate change. This downward mean value is also apparent in the fall season, according to the RCP4.5 scenario. However, there is an increasing mean value in other seasons. At locations 4 and 5, in winter, both RCP4.5 and RCP8.5 climate change scenarios suggest downward mean values, whereas in the other three seasons and for both climate change scenarios, there is an upward mean value. At location 6, the wave energy variation in all seasons and in both the RCP4.5 and RCP8.5 climate change scenarios is always increasing.

4.3. The bivariate probability distribution of occurrence and wave energy

In order to make accurate decisions regarding the appropriate locations for wave energy converter devices (WECs), it is necessary to consider probabilistic distributions for H_s and

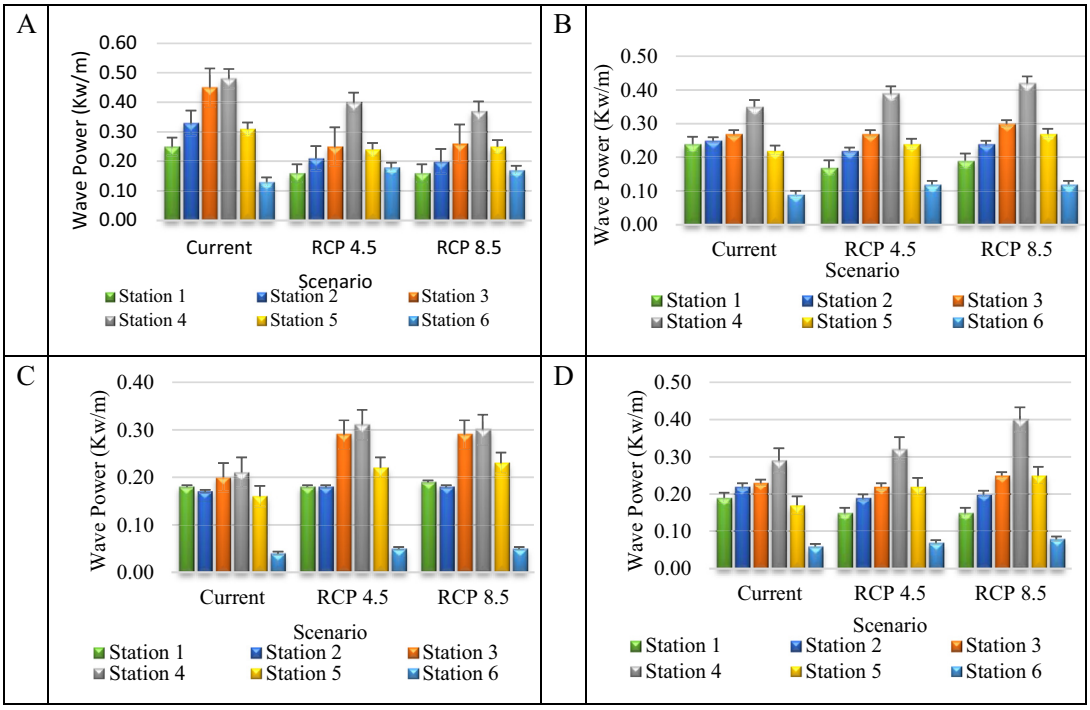

Figure 12 Mean values in wave energy changes at selected locations during winter for present climate conditions, as well as RCP8.5, and RCP4.5 climate change scenarios for 30 years (2070—2099); A) Winter, B) Spring, C) Summer, D) Fall.

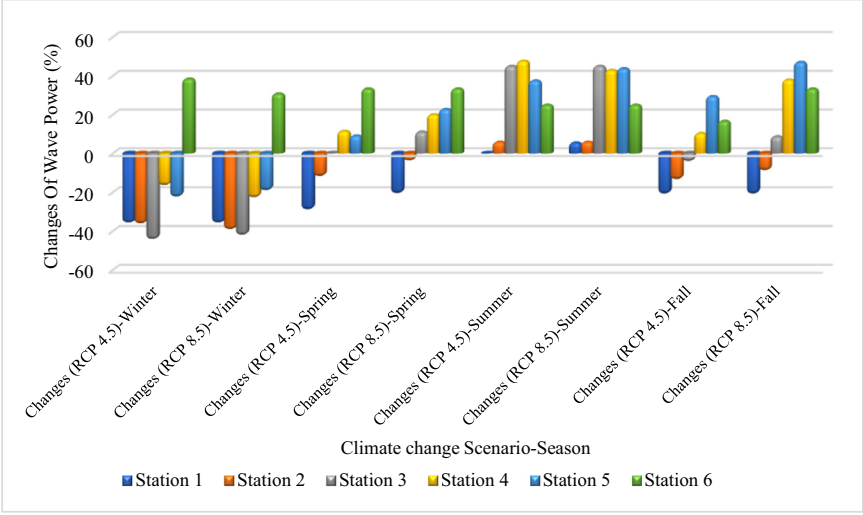

Figure 13 Changes of wave energy (%) for each season at selected station locations according to RCP8.5 and RCP4.5 climate change scenarios for 30 years (2070—2099).

T_e, which are used in most energy matrices in WEC calculations. The frequency of occurrence of each value for H_s and T_e in bivariate form is an expression of the prevailing wave characteristics at the associated point location. Figure 14 A—F describes the sea state conditions at the selected point locations, and the respective matrices are plotted for each of these locations.

As shown in Figure 14A, at location 1, the results are that for 41.5 and 38.1% of occasions, the wave periods are 2.5 s and significant wave heights are 0.2 and 0.4 m; thus the wave energy will be in the range of 0.12—0.33 kW/m. The occurrence of other wave periods and significant wave heights have occurrences that are less than 10%.

At point location 2 shown in Figure 14B, the wave periods are in the range of 1.5 to 3.5 s and significant wave heights, in the range of 0.2 to 0.6 m, with a higher probability of occurrence. The wave energy variation in these conditions is in the range of 0.1 to 0.96 kW/m.

At point location 3 shown in Figure 14C, the dominant results are wave periods of 2.5 s and significant wave heights in the range of 0.2—0.4 m. The amount of wave energy varies in the range of 0.11—0.31 kW/m.

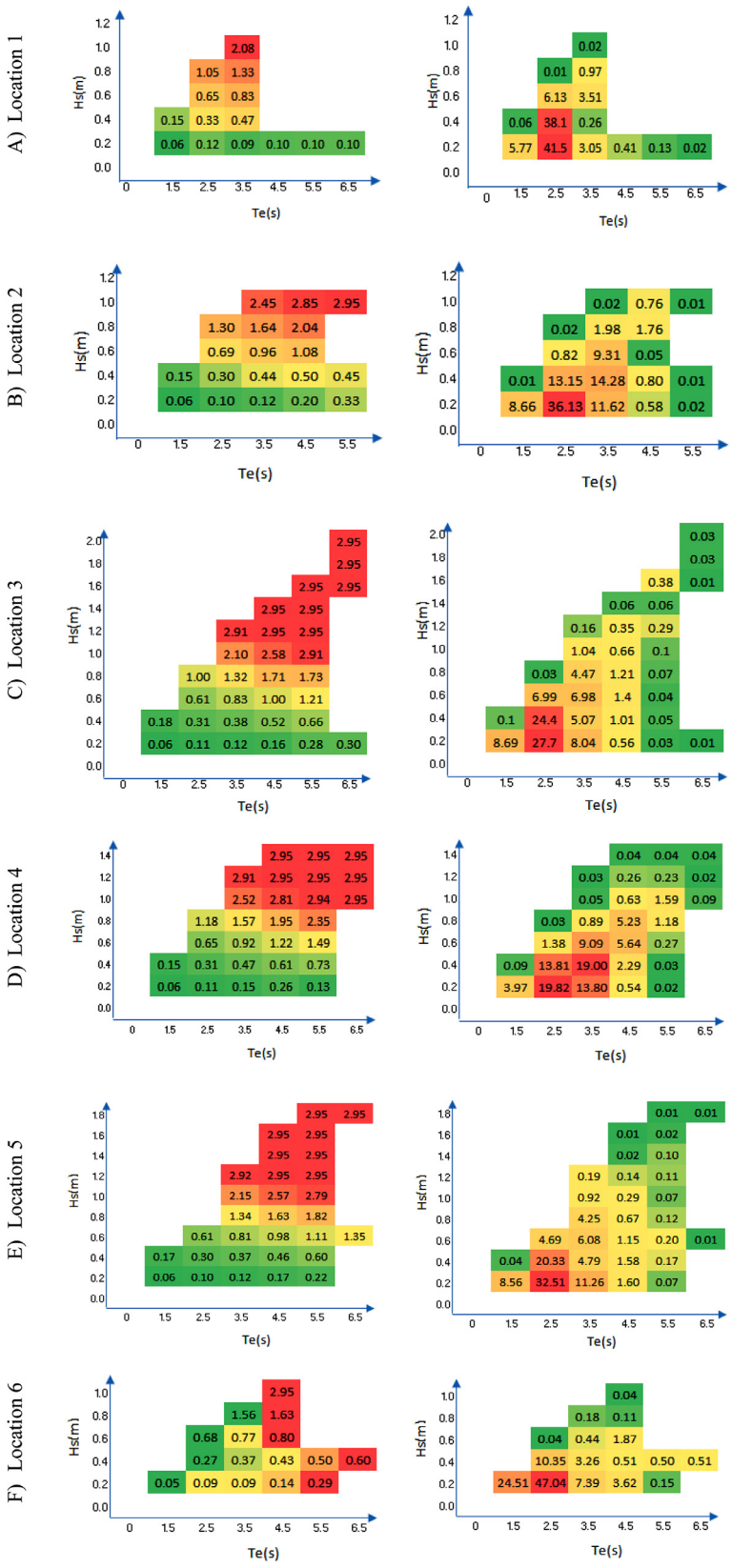

Figure 14 A, B, C, D, E and F: Bivariate distributions for the sea states H_s and T_e. The right panel represents the total of the occurrences and the left panel shows the average sea state wave energy for 30 years.

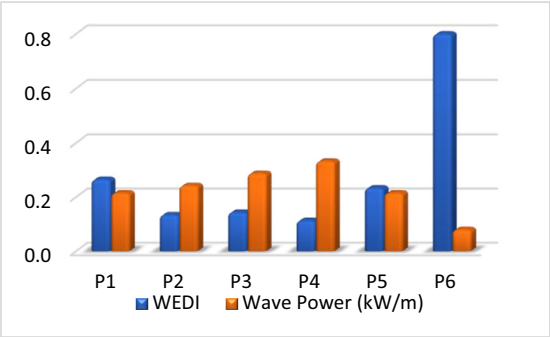

Figure 15 The comparison of WEDI and wave power at selected point locations.

At point location 4 shown in Figure 14D, the wave periods maximum occurrence is the range of 2.5—3.5 s and the significant wave heights in the range of 0.2—0.4 m. The change in wave energy in these conditions varies from 0.11 to 0.47 kW/m.

At the point location 5, based on Figure 14E, the maximum occurrence for wave periods is 2.5 s and significant wave heights are in the range of 0.2—0.4 m. The change in wave energy values in these conditions is from 0.1 to 0.3 kW/m.

Finally, at point location 6, as shown in Figure 14F, the maximum occurrence for wave periods is 2.5 s and significant wave heights are in the range 0.2—0.4 m. The change in wave energy in these conditions is between 0.09 to 0.27 kW/m.

Wave Energy Development Index

A significant parameter at the beginning of a wave energy development project is the wave energy development index (WEDI) value for a specific site. This index is obtained by dividing the average annual wave energy changes by the storm wave energy changes. It is dimensionless. The WEDI index distribution for the simulated 30 years is shown in Figure 15. This figure compares the WEDI index for selected locations. The highest WEDI index is suggested for location 6, and the lowest is for location 4. Our findings suggest that location 4 in the southern part of the Gulf is the most appropriate place to install wave energy converters.

5. Conclusions

The aim of this study is to investigate the characteristics of ocean wave parameters and wave energy potential, and the possible influence of climate change in the Persian Gulf region. Due to the high potential for energy extraction from wind-waves and advances in wave energy converter devices, waves are nowadays considered as an appropriate source for renewable energy. This is a new perspective compared to previous times. Iran has a huge potential source for this energy with approximately 2700 km of coastline along the northern and southern borders. The harnessing of this energy, in combination with other types of renewable energies such as solar energy, in which southern Iran abounds, can potentially turn the country from a dominant dependence on fossil fuels. Moreover, although some parts of the world ocean, such as the North Atlantic, and North and South Pacific, have a quite high wave energy values, more than 50 kW/m (Alcorn, 2013), in fact, many coastal areas like Italy (Vannucchi, and Cappietti, 2016), the Black Sea (Akpınar and Kömürcü, 2013), and North Coast of Australia (Hemer et al., 2017, 2018), have wave energy values that are less than 2 kw/m which is similar to our results. In the Persian Gulf similar study was conducted using present and future climates (A2, B1, and A1B scenarios), and the output maps showed that wave energy in coastal areas is less than 0.5 kW/m (Kamranzad, et al. 2015). The average wave power (kW/m) distribution in the Persian Gulf for a 25-year modeling period, 1984—2008, studied by Kamranzad et al. (2013), shows that done in the Persian Gulf shows the highest and lowest values of wave power were taken place in the central part and eastern part of the study area, respectively.

Computer model simulations for waves and climate change scenarios were performed. We compared present climate conditions in the Persian Gulf to future climate estimates.

We also estimated that most of the significant wave heights are less than one-meter high with wave periods that are less than 4.5 seconds. The results show that for location 1, 80%, of time T_e, H_s, and P_w vary between 2—3 s, 0.1—0.5 m, and 0.12—0.33 kW/m, respectively. For location 2, more than 50% of wave parameters including, T_e, H_s, and P_w, vary between 2—3 s, 0.1—0.5 m, 0.1—0.3 kW/m, respectively. In location 3, some 50 percent of wave parameters, T_e, H_s, P_w, vary 2—3 s, 0.1—0.5 m, and 0.11—0.31 kW/m, respectively. For location 4, more than 70% of T_e, H_s, and P_w change between 2—4 s, 0.1—0.5 m, 0.11—0.47 kW/m, respectively. For location 5, T_e, H_s, and P_w, in more than 50 percent of the time, vary between 2—3, 0.1—0.5, and 0.1—0.3 kW/m, respectively. In location 6, for more than 60% of the time, Te, Hs, and Pw change between 2—3 s, 0.1—0.5 m, and 0.09—0.27 kW/m, respectively. For locations 1, 2, 3, 4, 5, and 6 the value of WEDI are 0.27, 0.13, 0.14, 0.11, 0.23, and 0.80, as well as mean wave power (kW/m) for locations 1, 2, 3, 4, 5, and 6 are 0.22, 0.24, 0.29, 0.33, 0.22, and 0.08 kW/m, respectively.

According to these results, it appears that the potential energy level for waves in the southern part of the Persian Gulf is higher than in other areas. Based on our assessments, the locality around location 4 has emerged as having the most favorable conditions for wave energy extraction. There are no significant differences among locations 2, 3, and 5.

References

Aboobacker, V.M., Shanas, P.R., Alsaafani, M.A., Albarakati, A.M., 2017. Wave energy resource assessment for Red Sea. Renew. Energ. 114, 46—58.

Akpınar, A., Kömürcü, M.İ, 2013. Assessment of wave energy resource of the Black Sea based on 15-year numerical hindcast data. Appl. Energ. 101, 502—512.

Alcorn, R., 2013. Wave Energy. Future Energy: Improved, Sustainable and Clean Options for our Planet, 357—382.

Alizadeh, M.J., Alinejad-Tabrizi, T., Kavianpour, M.R., Shamshirband, S., 2020. Projection of spatiotemporal variability of wave power in the Persian Gulf by the end of 21st century: GCM and CORDEX ensemble. J. Cleaner Prod. 256, 120400. https://doi.org/10.1016/j.jclepro.2020.120400

Allen, M.R., Barros, V.R., Broome, J., Cramer, W., Christ, R., Church, J.A., Clarke, L., Dahe, Q., Dasgupta, P., Dubash, N.K., Edenhofer, O., 2014. IPCC fifth assessment synthesis report-climate change synthesis report. In: WMO, UNEP, IPCC, Geneva, Switzerland, 151 pp.

Alonso, R., Solari, S., Teixeira, L., 2015. Wave Energy resource assessment in Uruguay. Energy 93, 683—696.

Amirinia, G., Mafi, S., Mazaheri, S., 2017. Offshore wind resource assessment of Persian Gulf using uncertainty analysis and GIS. Renew. Energ. 113, 915—929.

Appendini, C.M, Urbano-Latorre, C.P., Figueroa, B., Dagua—Paz, C.J., Torres-Freyermuth, A., Salles, P., 2015. Wave Energy potential assessment in the Caribbean Low Level Jet using wave hindcast information. Appl. Energ. 137, 375—384.

Armanfar, M., Goharnejad, H., Niri, M.Z., Perrie, W., 2019. Assessment of coastal vulnerability in Chabahar Bay due to climate change scenarios. Oceanologia 61 (4), 412—426. https://doi.org/10.1016/j.oceano.2019.03.001

Besio, G., Mentaschi, L., Mazzino, A., 2016. Wave Energy resource assessment in the Mediterranean Sea on the basis of a 35-year hindcast. Energy 94, 50—63.

Breslow, P.B., Sailor, D.J., 2002. Vulnerability of wind power resources to climate change in the continental United States. Renew. Energ. 27 (4), 585—598.

Casas-Prat, M., Wang, X.L., Swart, N., 2018. CMIP5-based global wave climate projections including the entire Arctic Ocean. Ocean Model 123, 66—85.

DHI, M., 2005. spectral wave module—scientific documentation. Danish Hydraulic Institute.

Ertekin, R.C., Yingfan, X., 1994. Preliminary assessment of the wave-energy resource using observed wave and wind data. Energy 19 (7), 729—738.

Gallagher, S., Tiron, R., Whelan, E., Gleeson, E., Dias, F., McGrath, R., 2016. The nearshore wind and wave energy potential of Ireland: a high resolution assessment of availability and accessibility. Renew. Energ. 88, 494—516.

Goharnejad, H., Shamsai, A., Hosseini, S.A., 2013. Vulnerability assessment of southern coastal areas of Iran to sea level rise: evaluation of climate change impact. Oceanologia 55 (3), 611—637. https://doi.org/10.5697/oc.55-3.611

Hagerman, G., 2001. Southern New England Wave Energy Resource Potential. In: Proc. Building Energy Conf. 21 — 24 2001 March. Boston, USA.

Hemer, M.A., Manasseh, R., McInnes, K.L., Penesis, I., Pitman, T., 2018. Perspectives on a way forward for ocean renewable energy in Australia. Renew. Energ. 127, 733—745.

Hemer, M.A., Zieger, S., Durrant, T., O'Grady, J., Hoeke, R.K., McInnes, K.L., Rosebrock, U., 2017. A revised assessment of Australia's national wave energy resource. Renew. Energ. 114, 85—107.

Implementation Agreement on Ocean Energy Systems, 2007. Implementing agreement on ocean Energy systems (IEA-OES). Annual Rep. Internat. Energy Agency.

Jadidoleslam, N., Ozger, M., Agıralioglu, N., 2016. Wave power potential assessment of Aegean Sea with an integrated 15-year data. Renew. Energ. 86, 104—159.

Kamranzad, B., 2018. Persian Gulf zone classification based on the wind and wave climate variability. Ocean Eng 169, 604—635.

Kamranzad, B., Chegini, V., 2014. Study of wave energy resources in Persian Gulf: seasonal and monthly distributions. In: 11th Int. Conf. 'Coasts, Ports and Marine Structures'. Tehran, Iran.

Kamranzad, B., Etemad-Shahidi, A., Chegini, V., 2013. Assessment of wave energy variation in the Persian Gulf. Ocean Eng 70, 72—80.

Kamranzad, B., Etemad-Shahidi, A., Chegini, V., 2017. Developing an optimum hotspot identifier for wave energy extracting in the northern Persian Gulf. Renew. Energ. 14, 59—71.

Kamranzad, B., Etemad-Shahidi, A., Chegini, V., Yeganeh-Bakhtiary, A., 2015. Climate change impact on wave energy in the Persian Gulf. Ocean Dynam 65 (6), 777—794.

Kapelonis, Z.G., Gavriliadis, N., N, P., Athanassoulis, G.A., 2015. Extreme value analysis of dynamical wave climate projections in the Mediterranean Sea. Procedia Comput. Sci. 66, 210—219.

Korn, P., 2017. Formulation of an unstructured grid model for global ocean dynamics. J. Comput. Phys. 339, 525—552.

Kumar, V.S., Anoop, T.R., 2015. Wave energy resource assessment for the Indian shelf seas. Renew. Energ. 76, 212—219.

Langodan, S., Viswanadhapalli, Y., Dasari, H.P., Knio, O., Hoteit, I., 2016. A high-resolution assessment of wind and wave energy potentials in the Red Sea. Appl. Energ. 181, 244—255.

Liang, B, Fan, F, Yin, Z, Shi, H, Lee, D, 2016. Numerical modelling of the nearshore wave Energy resources of Shandong peninsula. China. Renew. Energ. 57, 330—338.

Liao, Y.P., Kaihatu, J.M., 2016. Numerical investigation of wind waves in the Persian Gulf: bathymetry effects. J. Atmos. Ocean. Technol. 33 (1), 17—31.

López, M., Veigas, M., Iglesias, G., 2015. On the wave Energy resource of Peru. Energ. Convers Manage. 90, 34—40.

Morim, J., Cartwright, N., Etemad-Shahidi, A., Strauss, D., Hemmer, M., 2014. A review of wave Energy estimates for nearshore shelf waters off Australia. Int. J. Marine Energ. 7, 57—70.

Neill, S.P., Hashemi, M.R., 2013. Wave power variability over the northwest European shelf seas. Appl. Energy 106, 31—46.

Neill, S.P., Lewis, M.J., Hashemi, M.R., Slater, E., Lawrence, J., Spall, S.A., 2014. Inter-annual and inter-seasonal variability of the Orkney wave power resource. Appl. Energ. 132, 339—348.

Ponce de León, S., Orfila, A., Simarro, G., 2016. Wave energy in the Balearic Sea. Evolution from a 29 year spectral wave hindcast. Renew. Energ. 85 (C), 1192—1200. https://doi.org/10.1016/j.renene.2015.07.076

Pous, S., Lazure, P., Carton, X., 2015. A model of the general circulation in the Persian Gulf and in the Strait of Hormuz: Intraseasonal to interannual variability. Cont. Shelf Res. 94, 55—70.

Riahi, K., Rao, S., Krey, V., Cho, C., Chirkov, V., Fischer, G., Kindermann, G., Nakicenovic, N., Rafaj, P., 2011. RCP 8.5—A scenario of comparatively high greenhouse gas emissions. Climat. Change 109 (1—2), art no. 33. https://doi.org/10.1007/s10584-011-0149-y

Rusu, E., Onea, F., 2013. Evaluation of the wind and wave energy along the Caspian Sea. Energy 50, 1—14.

Shanas, P.R., Aboobacker, V.M., Albarakati, A.M., Zubier, K.M., 2017. Climate driven variability of wind-waves in the Red Sea. Ocean Model 119, 105—117.

Thomson, A.M., Calvin, K.V., Smith, S.J., Kyle, G.P., Volke, A., Patel, P., Delgado-Arias, S., Bond-Lamberty, B., Wise, M.A., Clarke, L.E., Edmonds, J.A., 2011. RCP4. 5: a pathway for stabilization of radiative forcing by 2100. Climat. Change 109 (1—2), art. no 77. https://doi.org/10.1007/s10584-011-0151-4

Vannucchi, V., Cappietti, L., 2016. Wave energy assessment and performance estimation of state of the art wave energy converters in Italian hotspots. Sustainability 8 (12), 1300. https://doi.org/10.3390/su8121300

Vieira, F., Cavalcante, G., Campos, E., 2020. Analysis of wave climate and trends in a semi-enclosed basin (Persian Gulf) using a validated SWAN model. Ocean Eng 196, 106821. https://doi.org/10.1016/j.oceaneng.2019.106821

Wang, Z., Dong, S., Li, X., Guedes-Soares, C., 2016. Assessments of wave energy in the Bohai Sea, China. Renew. Energ. 90, 145—156.

WCRP Global Sea Level Budget Group, 2018. Global sea-level budget 1993—present. Earth Sys. Sci. Data 10, 1551—1590. http://dx.doi.org/10.5194/essd-10-1551-2018

Zhou, G., Huang, J., Yue, T., Luo, Q., Zhang, G., 2015a. Temporal-Spatial distribution of wave Energy: A case study of Beibu Gulf, China. Renew Energ. 74, 344—356.

Zhou, G., Huang, J., Zhang, G., 2015b. Evaluation of the wave Energy conditions along the coastal waters of Beibu Gulf, China. Energy 85, 449—457. https://doi.org/10.1016/j.energy.2015.03.094